Chapter 2

Executive Summary

The thrust of experiments proposed for the CLAS^{++} detector in conjunction with the 12 GeV CEBAF accelerator is the study of the nucleon through exclusive and semi-exclusive processes. This will provide new insights into the nucleon dynamics at the elementary quark and gluon level. The internal structure of the nucleon has been studied primarily during the past three decades through the *inclusive* scattering of high-energy leptons off the nucleon in the regime of "Deeply Inelastic Scattering" (DIS). When one sums over all possible hadronic final states, simple theoretical interpretations can be obtained in the framework of the parton model.

Inclusive measurements are largely insensitive to the internal quark-gluon dynamics, i.e. the nucleon wave function. They essentially reveal a one-dimensional image of the quark longitudinal momentum distribution. Now with the prospects of a new high-energy, high-luminosity, and continuous electron beam provided by the 12 GeV upgrade of CEBAF, a wide variety of *exclusive* processes in the Bjorken regime will become accessible experimentally when employing the large acceptance CLAS^{++} detector system in Hall B. Measurement of these processes will allow us to access the full internal dynamics of the nucleon through correlations of their elementary constituents, quarks and gluons.

The tables at the end of this chapter provide an overview of the physics topics and reactions that can be studied with CLAS^{++}. In the following sections we briefly address some of the major physics topics.

2.1 Quark-Gluon Dynamics and Nucleon Tomography

Until recently, very few exclusive processes could be treated in the framework of perturbative QCD and compared to experimental data. The recently developed formalism of Generalized Parton Distributions (GPDs) now holds promise to extend theoretical interpretations exclusive processes of the electroproduction of photons,

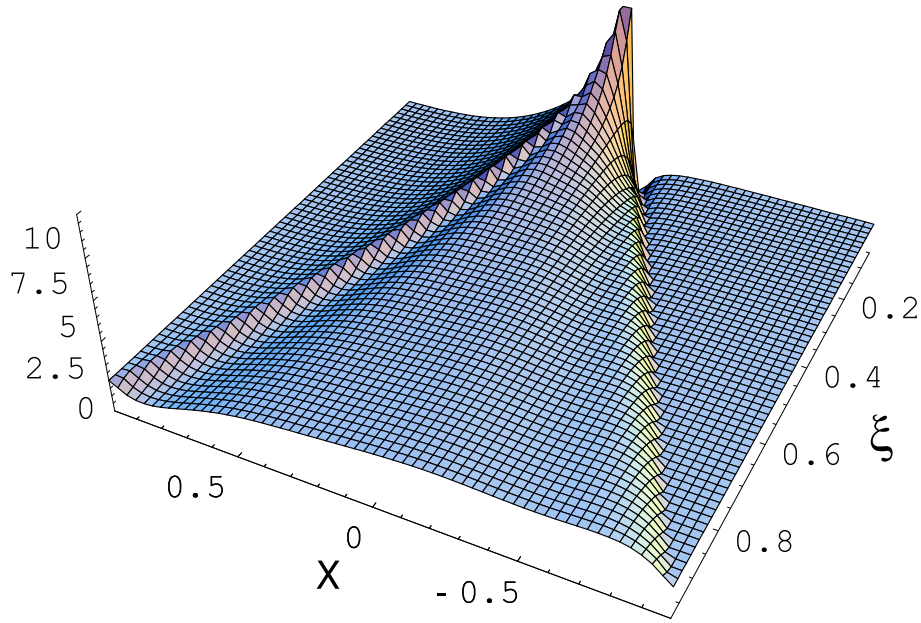

Figure 2.1: Model representation of the GPD $H(x, \xi, t = 0)$ in two dimensions. The known parton momentum densities constrain the distribution at $\xi = 0$. The new physics is contained in the ξ dependence and the t-dependence of this surface, which can currently only be modeled. The dramatic change in the shape of the surface reflects the change in the underlying physics. As ξ increases the correlations between the quarks and anti-quarks increase leading to meson-like distributions at large ξ.

vector mesons, and pseudoscalar mesons off the nucleon. GPDs encompass the standard forward-parton distribution functions, measured for instance in deeply inelastic scattering, elastic and resonance transition form factors, and the full complexity of two-parton correlations. Figure 2.1 shows a model representation of the GPD $H(x, \xi, t)$. Currently, only the distribution at the edge $H(x, 0, 0)$ is known from DIS experiments. A first foray into the realm of the new physics has been made. Measurements with CLAS at 4.3 GeV have demonstrated that the physics of GPDs can be accessed in the case of Deeply Virtual Compton Scattering (DVCS) already at lower energies[13]. Figure 2.2 shows projected data of a measurement of the DVCS process via the beam spin asymmetry using CLAS^{++}. The entire set corresponds to about 1000 data points that are measured simultaneously, and cover the entire kinematic range accessible with an 11 GeV polarized electron beam. Figure 2.3 illustrates the broad kinematic coverage of the proposed DVCS measurements. It shows the DVCS beam spin asymmetry for some bins in ξ (or Bjorken x_B) and Q^2 versus the momentum transfer t to the proton that are measured simultaneously. The graphs also show the sensitivity to different parameterizations of the GPDs.

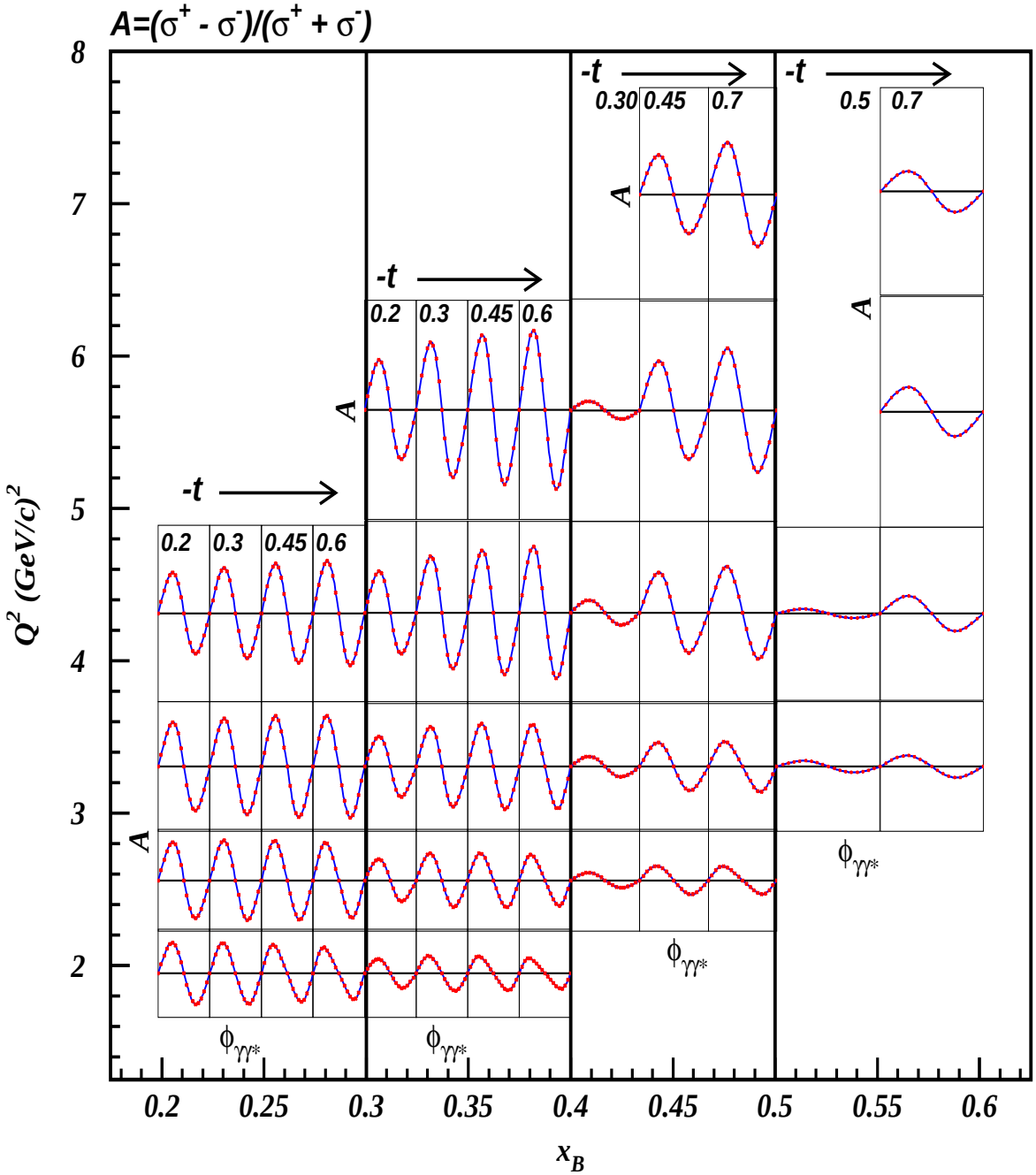

Figure 2.2: Beam spin asymmetry for $\vec{e}p \to ep\gamma$. Projected data with an upgraded CLAS and an 11 GeV electron beam for kinematic bins that are measured simultaneously. Complete azimuthal distributions in over 50 bins in Q^2, ξ, t will be collected simultaneously in 2000 hours of beam time. The curves represent a specific model for the GPDs. At the same time the DVCS cross section differences will be measured as well. In kinematics where the DVCS cross section is large, absolute cross section measurements will be possible.

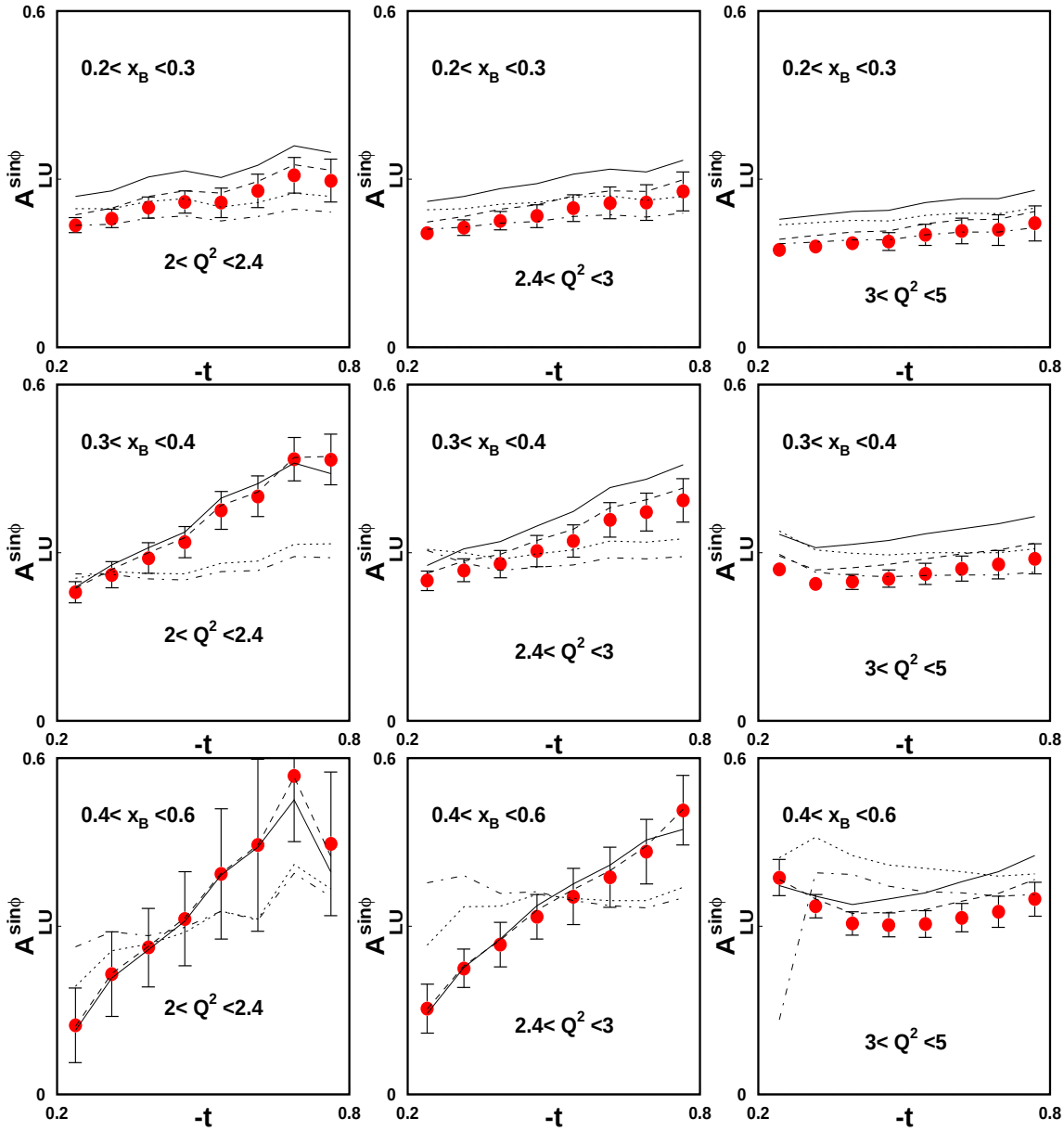

Figure 2.3: Momentum transfer-dependence of the beam spin asymmetry for $\vec{e}p \to ep\gamma$. Projected data with an upgraded CLAS and an 11 GeV electron beam for kinematic bins that are measured simultaneously. The curves represent different model parameterizations for the GPDs.

Complementary information with different sensitivities to GPD parameterizations can be obtained in measurements using polarized hydrogen (NH_3) targets. In order to separate all 4 leading twist GPDs in DVCS measurements with polarized targets are needed as well. At somewhat higher Q^2, other final states including ρ and ω vector mesons, and π^0 and η (Deeply Virtual Meson Production, DVMP) will provide information that is complementary to DVCS, allowing for an unraveling of the flavor and spin composition of the GPDs. These processes will be measured simultaneously with the DVCS beam spin asymmetry, the differential cross sections, and helicity-dependent cross section differences. Kinematic coverage will also be similar.

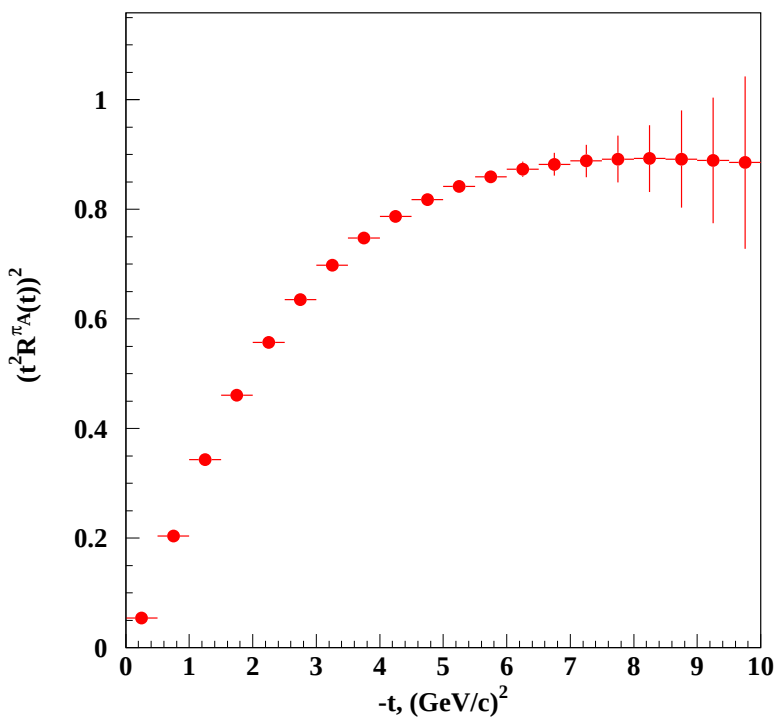

Figure 2.4: Simulated extraction of the form factor $(t^2 R_A^{\pi^0})^2$ from Eq. 3.24 compared with theory[14, 15].

Another important component of our GPD program will be to measure exclusive deeply virtual meson and photon production in the *high t - low* Q^2 regime, simultaneously with our measurements at *low t - high* Q^2. These reactions will provide x^{-1} moments for the small $b_\perp$ components of the correlations function, and combined with the $m = 0$ moments obtained in the high Q^2 form factor measurements will give powerful constraints on the nucleon's short distance parton wave functions. $R_A^{\pi^0}(t)$ is the axial form factor which is composed of the spin dependent GPDs as follows:

$$R_A^{\pi^0}(t) \sim (e_u R_A^u - e_d R_A^d)$$

$$R_A^q(t) = \int_{-1}^{1} \frac{dx}{x} \tilde{H}^q(x, 0, t)$$

$\tilde{H}^q(x, \xi, t)$ is the GPD function for quark of flavor q.
Thus, the key ingredients of the reaction which are probed are the GPDs $\tilde{H}^q(x, 0, t)$, with $H^q(x, 0, 0) = \Delta q(x)$, the pion distribution function $\phi_M(\tau)$, and the single quark hard scattering amplitude $f_0^{(q)}(\tau, s, Q^2, t)$. Figure 2.4 shows projected data for a measurement of the formfactor $R_A^{\pi^0}$ in exclusive π^0 production at high t.

In conclusion, the complete extraction of the GPDs represents an extensive program, rather than a single experiment, involving the measurement of a variety of channels and observables over a broad kinematic range.

The necessity to measure exclusive reactions at high photon virtualities and low momentum transfer to the target nucleon, as well as at low photon virtualities and high momentum transfer, is driving the CLAS upgrade.

While the GPD program is the flagship program for CLAS^{++}, there are several other programs and measurements of great importance for our understanding of the nucleon's valence quark structure that can be done best utilizing the large acceptance of CLAS^{++}. Several of them are briefly described in the following sections, others are described in the physics sections.

2.2 Valence Quark Distribution and Hadronization

2.2.1 The Proton and Neutron Spin Structure

CLAS has been used to measure the spin structure function $A_1(x, Q^2)$ for protons and deuterons through and beyond the nucleon resonance region, in the Q^2 range from 0.15 - 2 GeV^2. From these data the structure function $g_1(x, Q^2)$ and its first moment $\Gamma_1(Q^2) = \int g_1(x, Q^2)dx$ have been extracted using parameterizations of the unmeasured deeply inelastic part at small x. The upgrade will allow a large extension in the x and Q^2 range. The large x regime is crucial for determining higher moments such as $\int x^2 g_1(x, Q^2)dx$. Moments are needed for a QCD analysis using the operator product expansion of QCD, which will elucidate the importance of "higher twist" effects (strong quark-gluon correlations) in the nucleon. It will also expose the dynamics underlying the quark-hadron duality and the nature of the resonance-scaling transition. Figure 2.5 shows projected data for $A_{1p}(x)$ in the deeply inelastic regime. Data with similar coverage in x will be obtained for the deuteron (neutron). If "duality" arguments apply namely if data in the resonance region approximately average to the DIS data, the x range can be extended to $x = 0.95$.

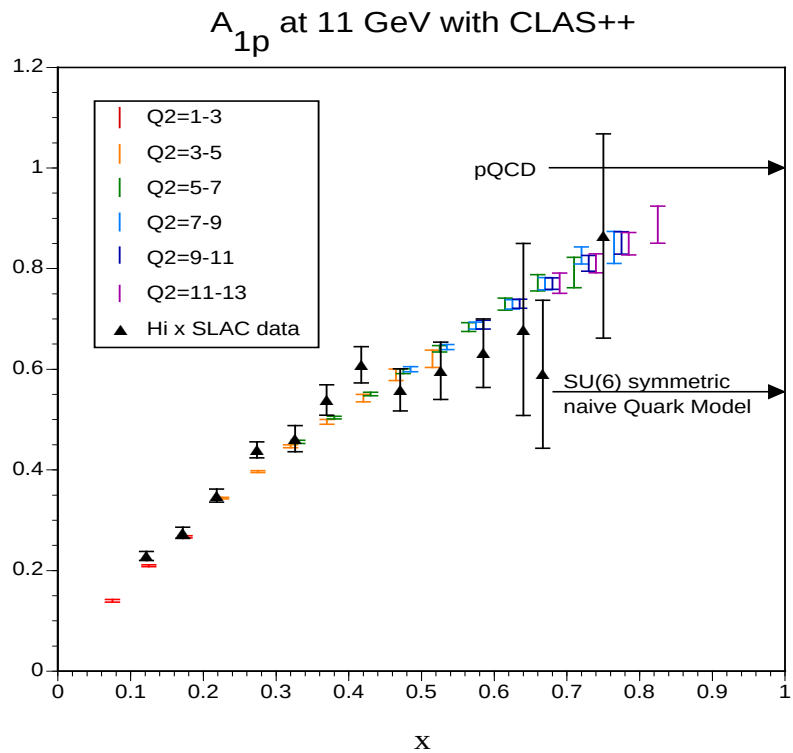

Figure 2.5: Projected CLAS^{++} data at 11 GeV for the helicity asymmetry $A_{1p}(x)$ of the proton. The x range may be extended to 0.95 if duality arguments hold. The arrows at $x \to 1$ indicate the pQCD limit of $A_{1p} = 1$, and the $SU(6)$ limit of $A_{1p} = 5/9$, respectively. The color code shows that measurements at fixed x are done at different Q^2 allowing to test for a possible Q^2 evolution.

.

2.2.2 Tagged Quark Distribution Function

Semi-inclusive processes such as $eA \to eMX$, where $A = p,\ d,\ {}^3$He,..., and $M = \pi,\ \eta,\ K,\ \rho,\ \omega$ are powerful tools to tag the flavor of the struck quark, and in conjunction with polarized beams and polarized targets, to probe the quark spin distributions in nucleons and nuclei. Recent CLAS data[16] on the beam spin asymmetry in $\vec{e}p \to e\pi^+X$ indicate that factorization of the parton distribution functions and the quark fragmentation functions may already be valid at present JLab energies, provided the pion carries most of the energy of the virtual photon. Given approximate factorization, measurements of beam and target spin asymmetries in the 12 GeV energy range will probe the quark transverse spin distribution, and will also be sensitive to the quark-gluon final state interaction.

The semi-inclusive double polarization asymmetries with a longitudinally polarized target (σ_{LL}) have been the subject of considerable interest recently, both theoretically and experimentally. While the polarized u-quark distribution is reasonably well established experimentally, the polarized d-quark distribution is poorly known,

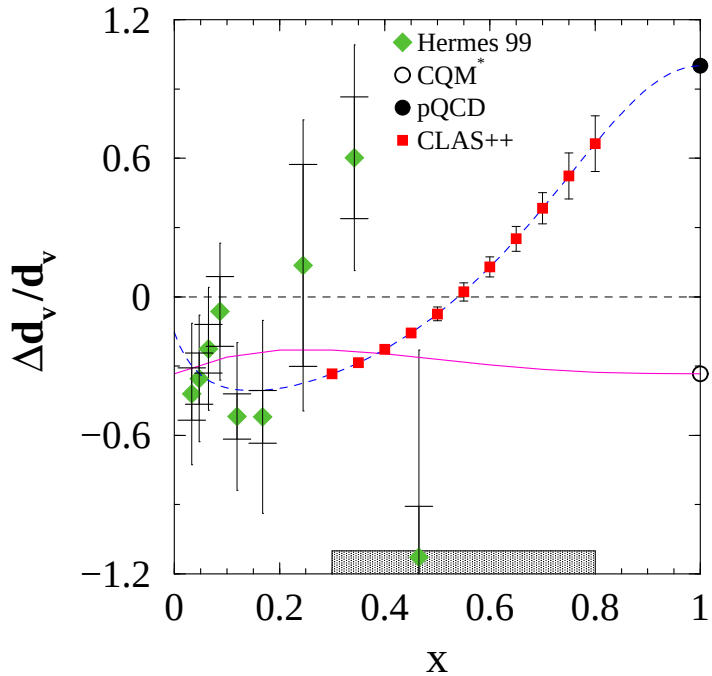

Figure 2.6: Projected data for the valence d-quark helicity distribution with CLAS^{++} from semi-exclusive pion production using a polarized beam and a longitudinally polarized target. Higher x values can be reached if duality arguments apply. In this figure, 1000 hrs of data taking with a NH_3 target and 1000 hrs with a ND_3 have been assumed. The double error bars on the existing data points represent the statistical (inner) and the total (statistics and systematics) errors. The curves represent two models of the x dependence. The shaded area at the bottom shows the expected systematic error of the measurement.

especially at large x, where there are significant differences between model predictions. The data shown in Fig. 2.6 represent the present knowledge of Δd at large x. CLAS^{++} will allow measurements in the x region above 0.5. Good particle identification is needed for a successful program to study semi-inclusive reactions.

2.2.3 Novel Quark Distributions

Apart from GPDs, there is another class of nonperturbative functions that carry information not only on longitudinal but also on transverse hadron structure. These are the transverse momentum dependent (TMD) parton distributions [17, 18, 19, 20, 21, 22, 23, 24] containing direct information about the quark orbital motion [25, 26, 24]. TMD distributions in impact parameter space are correlation functions for the transverse distance of a single parton with respect to all other partons in the wave function [27]. This is in contrast to GPDs (integrated over the transverse momentum) where the relative distance of partons to each other in a hadron stays the same. The TMDs appear in azimuthal moments of double-polarized cross sections in single-hadron production in DIS [20, 21]. As shown recently in Ref.[23], the interaction of active partons

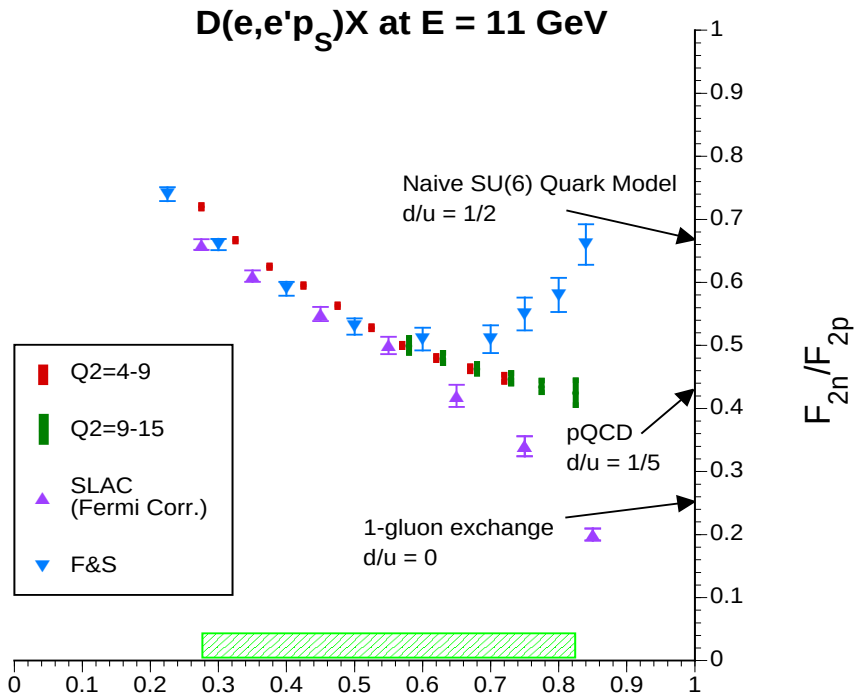

Figure 2.7: Projected CLAS^{++} data at 11 GeV for the ratio of the neutron to proton structure functions F_{2n}/F_{2p}. The read and green symbols are measurements at fixed x but different Q^2 taken simultaneously. This allows checking for a possible Q^2 evolution. The other symbols are from previous SLAC measurements interpreted with different nuclear models, indicating strong model-dependence at large x. The x range may be extended to 0.95 if duality arguments can be used.

in the hadron with the target spectators [25, 28] leads to gauge-invariant TMD parton distributions. A non trivial phase structure of QCD amplitudes due to rescattering results in *time-reversal odd* (T-odd) effects and the appearance of single-spin asymmetries at leading twist[25, 26]. The list of novel physics observables accessible in SSAs includes the chiral-odd distribution functions, such as the transversity [29, 30], the *time-reversal odd* fragmentation functions, in particular the Collins function [19], and the recently introduced [18, 22, 25, 26, 28] *time-reversal odd* distribution functions (Sivers function). Measurements of single-spin asymmetries in semi-inclusive DIS at CLAS^{++} with longitudinally and transversely polarized targets will accomplish separation of contributions from all these functions.

2.2.4 The Neutron Structure Function $F_{2n}(x, Q^2)$

New opportunities arise with the upgrade to directly determine the $F_{2n}(x, Q^2)$ structure function of the neutron for the first time in the large x region. Using a deuteron gas target, the recoil spectator proton (p_s) in the reaction $ed \to ep_sX$ can be mea-

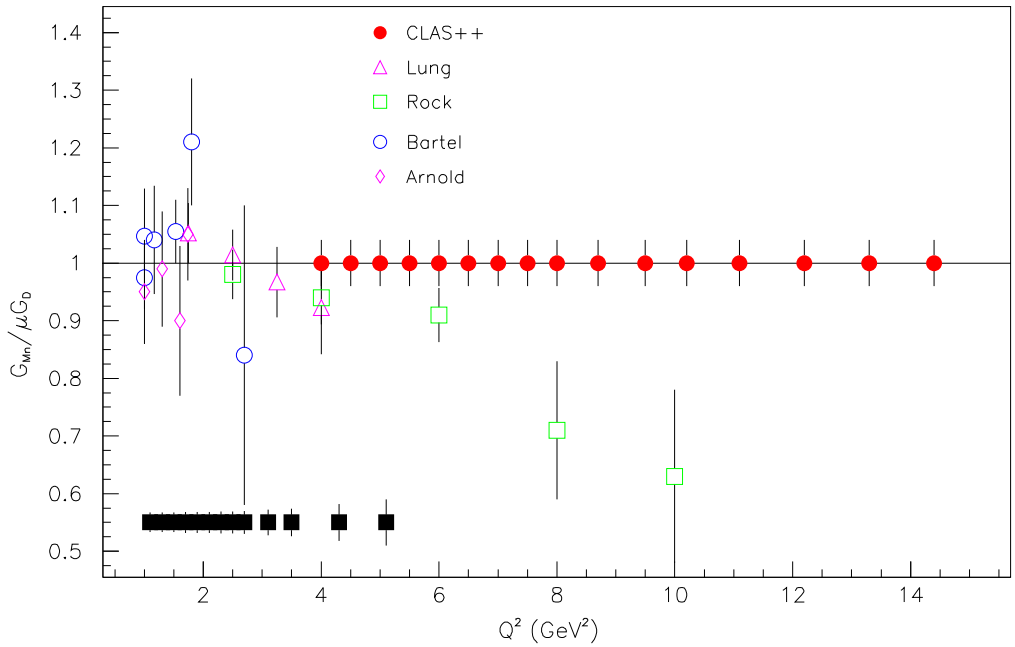

Figure 2.8: Projected CLAS^{++} data at 11 GeV for the neutron magnetic formfactor. The points at the lower left of the panel are projected errors of the existing CLAS data which are currently being analyzed. The open symbols are data from measurements at SLAC and at DESY

sured using a low-density gas detector. Recoil proton momenta as low as 80 MeV/c can be detected, allowing direct verification that the process has taken place on an almost-free neutron of known momentum. Low luminosity operation and the large acceptance of CLAS are crucial to reduce accidentals from quasi-real photoproduction events. Expected results are shown in Fig. 2.7.

2.2.5 Space-Time Characteristics of Hadronization

The hadronization process, which is the primary manifestation of confinement in QCD, has been studied at length for decades. While many features of this fundamental process are well-reproduced using phenomenological modeling, little direct experimental information is available on its space-time characteristics. Information of this type can be obtained by studying the modification of quark fragmentation functions within the nuclear medium. Recent exploratory measurements have offered tantalizing hints as to how the hadronic formation time varies with the size or mass of the quark system being formed, finding, for example, that the proton formation time is more than twice as long as that for charged pions[31][32]. However, these pioneering studies are limited to $Q^2 \approx 1-2$ GeV^2, and to just a few hadron types, by the available luminosity. With the advent of CLAS^{++}, a ground-breaking advance in such studies will become possible. A broad program of measurements using a score

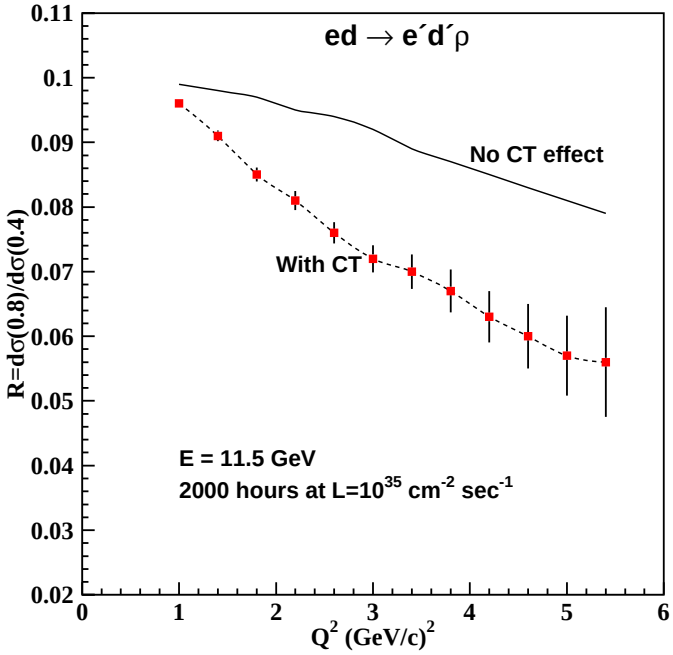

Figure 2.9: Expected errors on the cross section ratio for coherent ρ° production off deuterium at $-t = 0.4$ and 0.8 (GeV/c)^2 for 2000 hours of running at a luminosity of 10^{35}cm^{-2}sec^{-1}.

of mesons and baryons (see the table in Section 3.4.2) will systematically map out the dependence of the hadron formation time as a function of Q^2, ν, p_T, z, helicity, hadron mass and size, and quark flavor. A program of this breadth can only be carried out with a large acceptance spectrometer at high luminosity. Accompanying the hadronization analysis will be an investigation of quark energy loss, and a comprehensive array of color transparency studies via vector meson production and quasielastic scattering. The analysis of such a data set will yield a wealth of new insights into the nature of the hadronization process, which is a direct manifestation of confinement in QCD. Figure 2.9 shows an example of the expected effect for coherent ρ° production off deuterium with and without the inclusion of color coherent effects.

2.3 Form Factors and Resonance Excitations

2.3.1 The Magnetic Structure of the Neutron

The electric and magnetic form factors of the neutron are the major missing pieces in the elastic form factor analysis of the nucleon charge and magnetization distributions. An experiment with CLAS at 4 GeV is using the cross section ratio of the processes $ed \to enX$ and $ed \to epX$ to precisely measure the magnetic form factor $G_{Mn}(Q^2)$ up to Q^2 =5 GeV^2[33]. With the upgrade this quantity can be measured up to Q^2=14 GeV^2 in CLAS^{++}. Projected data are shown in Fig. 2.8.

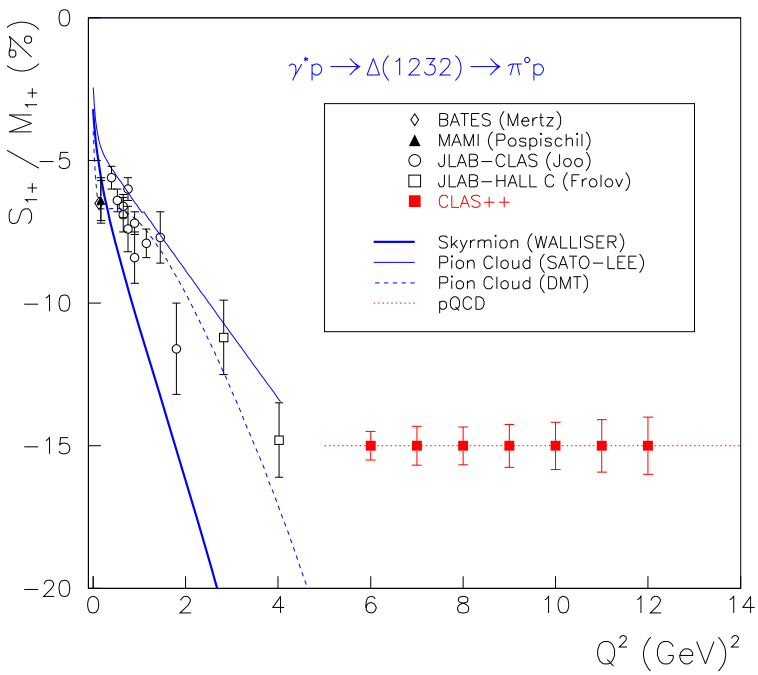

Figure 2.10: Ratio R_{SM} for the $N - \Delta$ transition. The data points at lower Q^2 are from CLAS and Hall C. The high Q^2 points correspond to projected error bars for a measurement with CLAS^{++}.

2.3.2 Resonance Excitation Dynamics

The current CLAS program is providing accurate information on resonance transition form factors for Q^2 up to 4 - 6 GeV^2. Much effort has gone into the measurement of the multipole ratio $R_{EM} = E_{1+}/M_{1+}$ for the $N - \Delta(1232)$ transition[34, 35]. R_{EM} is predicted to approach +1 asymptotically, while the ratio is nearly flat at -0.02 for $Q^2 < 4$ GeV^2 with no clear trend towards the asymptotic value. In addition we measure the longitudinal ratio $R_{SM} = S_{1+}/M_{1+}$ that exhibits an approximately linear dependence with Q^2. R_{SM} is easier to measure than R_{EM} as $|R_{SM}|$ rises with Q^2. As pQCD predicts a constant value for R_{SM} at large Q^2, a change towards a flatter Q^2 dependence may indicate the onset of significant leading-order pQCD contributions. With CLAS^{++} this measurement can be extended to $Q^2 = 12$ GeV^2 where indication of a transition to pQCD behavior may set in. Figure 2.10 shows the projected data.

Some of the higher-mass states are expected to become more prominent with increasing Q^2, opening up the possibility for a "hard" N^* spectroscopy, where connections to pQCD may be possible. At 4 GeV, measurements in the $p\pi^+\pi^-$ channel show a dramatic rise of the $P_{13}(1720)$ resonance strength with Q^2 in comparison with non-resonant contributions. With CLAS^{++} these measurements may be extended from $Q^2 = 1.5$ GeV^2 to $Q^2 > 4$ GeV^2. The program on hard N^* spectroscopy requires the full acceptance of CLAS^{++} for both the detection of photons and of charged particles.

2.4 The Detector

The CLAS^{++} detector is shown in Fig. 2.11. It meets the basic requirements of the physics program currently anticipated for the 12 GeV upgrade.

The main features of CLAS^{++} are:

- High operating luminosity of $10^{35}\text{cm}^{-2}\text{s}^{-1}$ for hydrogen targets, a ten-fold increase over current CLAS operating conditions.
- Improved detection capabilities for forward-going high momentum particles. Charged particles that bend outwards in the torus field can be reconstructed for angles as low as 5 degrees. Photon detection will be possible for angles as low as 3 degrees. Acceptances for electrons are momentum-dependent, and range from about 8 degrees to 40 degrees.
- Capability to detect the recoil baryons at large angles.
- Larger momentum range for the separation of electrons, pions, kaons, and protons. This is achieved with better resolution time-of-flight counters, and with the installation of a new gas Cerenkov detector.
- Improved hermeticity for the detection of charged particles and photons in regions where CLAS currently has no detection capabilities, achieved by instrumenting the coil regions and by extending the polar angle range for photon detection to 135 degrees.

CLAS^{++} makes use of many of the components of the current CLAS detector.

- The torus magnet will be re-used in a slightly modified form.
- All large forward calorimeters will be used for electron, photon, and neutron detection.
- All gas Cerenkov counters will be used with adjustments in the optics and replacement of 1/3 of the mirrors.
- The time-of-flight scintillator material will be used to make smaller scintillator slabs for better timing.
- Part of the CLAS drift chamber electronics will be re-used.

A major new component in CLAS^{++} is the Central Detector. Its main component is a superconducting solenoid magnet, which has a dual function: It replaces the existing mini-torus for shielding of the Møller electrons, and it provides the magnetic field for the momentum analysis of charged particles at large angles. Time-of-flight

scintillators are used to provide particle identification at scattering angles greater than 40 degrees. Due to the limited space available excellent timing resolution is essential. Tracking at large angles is provided by a combination of drift chambers with cathode strip readout and a microstrip detector near the vertex. Since most charged tracks will have momenta of 1 GeV/c or less sufficient momentum resolution can be achieved even in the limited space available for tracking. A compact electromagnetic calorimeter based on tungsten powder and scintillating fiber technology provides photon detection capability for the angle range from 40-135 degree.

Much of the instrumentation of CLAS will be re-used in the CLAS^{++} Forward Detector (FD). However, some modifications and additional detectors are needed in the Forward Detector as well. The main new component is a threshold gas Cerenkov counter for pion detection. CO_2 is considered as radiator gas. The light collection is accomplished using a mirror system that focuses the Cerenkov light onto photomultipliers located sideways of the torus magnet. This area will be accessible after the removal of the CLAS drift chambers. The Cerenkov counter will allow electron and pion identification up to nearly 5 GeV/c. Beyond 5 GeV/c electrons are identified in the forward electromagnetic calorimeter. There is also additional electromagnetic calorimetry placed in the area of the torus coils for improved hermiticity. Lead-tungstate crystals have emerged as a good choice for this detector.

A pre-shower detector will be inserted in front of the existing CLAS electromagnetic calorimeters. This detector will allow separation of single photons from $\pi^0 \to \gamma\gamma$ events especially needed for deeply virtual Compton scattering.

All drift chambers in CLAS will be replaced by new ones that will cover a smaller angle range with a factor of two smaller cell sizes to reduce the accidental hit occupancy due to photon interactions allowing for a corresponding gain in luminosity.

The existing forward detection system will be modified to extend particle identification and reconstruction to higher momenta. This will be accomplished by several means: The timing resolution of the scintillation counters will be improved by using smaller scintillator slabs, and by adding an additional layer of scintillators, and by replacing the PMTs by new ones with better timing characteristics. This is expected to improve the timing resolution to about 60 psec. The existing gas Cerenkov counter will be modified for improved pion detection capabilities for momenta greater than 2.7 GeV/c. .

With these modifications and additions to the existing CLAS components, CLAS^{++} will be able to carry out the core program for the study of the internal nucleon dynamics and hadronization processes by measuring exclusive, semi-inclusive, and inclusive processes.

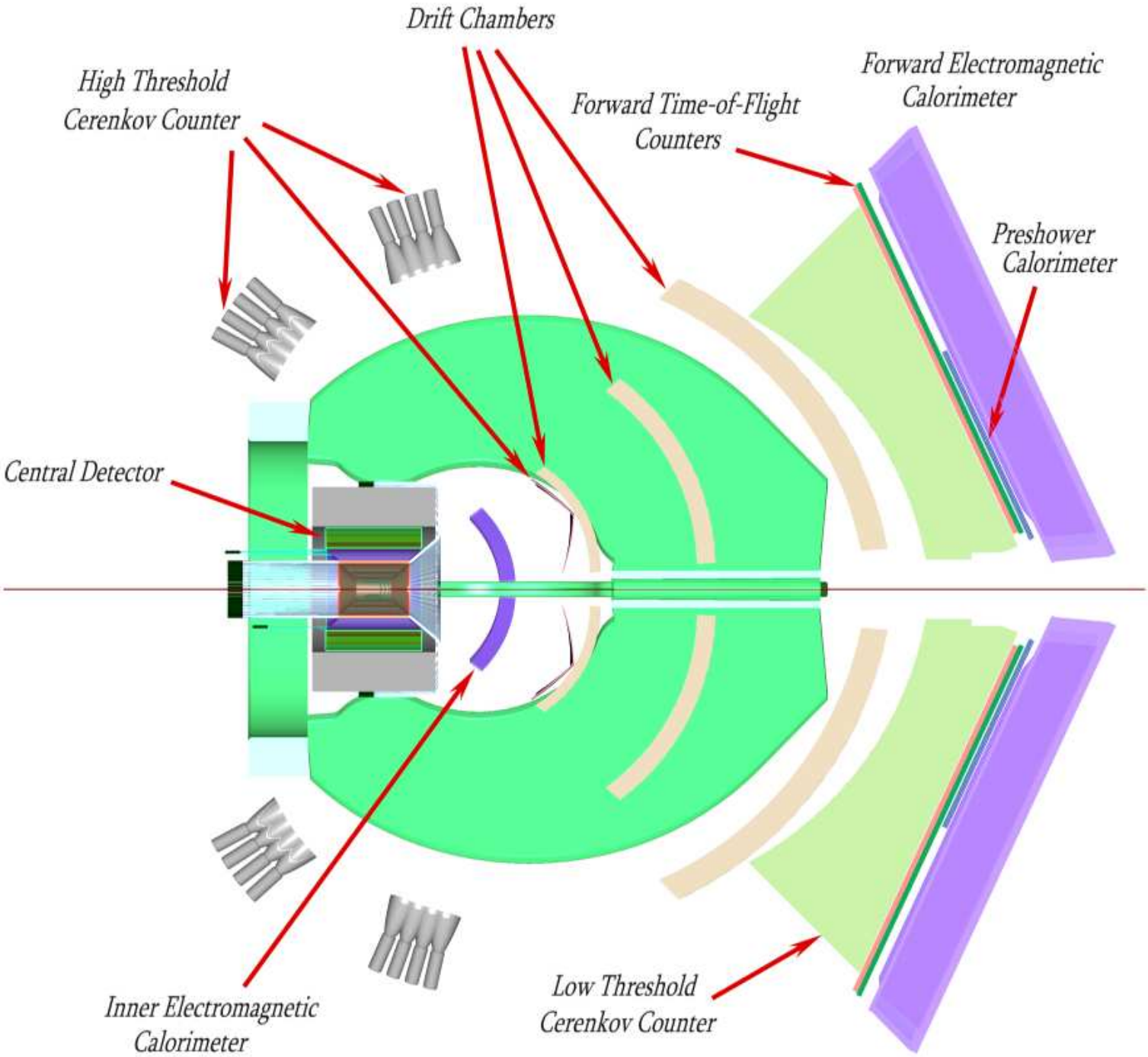

Figure 2.11: The upgraded CLAS^{++} detector.

Table 2.1: **CLAS^{++} PROGRAM SUMMARY - NUCLEON QUARK-GLUON DYNAMICS**
The color code indicates reactions that will be measured simultaneously in CLAS^{++}.

PHYSICS PROGRAM	**REACTION(s)**	**OBSERVABLES**	**REQUIREMENTS**
EXCLUSIVE REACTIONS AND GPDs			**Large Q^2, X_B, t, ϕ**
Deeply Virtual Compton Scattering(DVCS) Proton dynamics and tomography	$\vec{e}p \rightarrow ep\gamma$ $\vec{e}\vec{p} \rightarrow ep\gamma$ $\vec{e}p^T \rightarrow ep\gamma$	GPDs(H), $\xi = x$ GPDs($\tilde{H}$), $\xi = x$ GPDs($\tilde{E}$), $\xi = x$	Pol. Beam Long pol. target Trans. pol. target
Hard vector meson production Spin Filtering and flavor decomposition	$\vec{e}p \rightarrow ep(\rho,\omega,\phi)$ $\vec{e}\vec{p} \rightarrow ep(\rho,\omega,\phi)$ $\vec{e}p^T \rightarrow ep(\rho,\omega,\phi)$	GPDs and angular momentum	Multi-particle detection
Hard pseudoscalar meson production Structure of the proton at small distances	$\vec{e}p \rightarrow eN(\pi^0,\eta,\pi^+)$ $\vec{e}\vec{p} \rightarrow eN(\pi^0,\eta,\pi^+)$ $\vec{e}p^T \rightarrow eN(\pi^0,\eta,\pi^+)$	GPDs at low and high t	Multi-photon detection Large angular coverage Large t
Double DVCS (DDVCS) Δ and N^* DVCS	$\vec{e}p \rightarrow epe^+e^-$ $\vec{e}p \rightarrow ep(\Delta,N^*)\gamma$	GPDs at $-\xi < x < \xi$	Multi-particle detection
INCLUSIVE VALENCE QUARK STRUCTURE FUNCTION			**Low luminosity program**
Neutron structure function Novel method to study neutron dynamics	$\vec{e}D \rightarrow ep_sX$ $\vec{e}D \rightarrow ep_s(\pi^-p),\Delta^+\pi^-$	d/u ratio	Neutron tagging Low $L \rightarrow$ large acc.
Nucleon spin structure function	$\vec{e}\vec{p} \rightarrow eX$, $\vec{e}p^T \rightarrow eX$ $\vec{e}\vec{D} \rightarrow eX$ $\vec{e}D^T \rightarrow eX$	A_1^P, g_2^p, moments A_1^n , g_2^n, moments	Low $L \rightarrow$ large acc. Pol. targets
SEMI-INCLUSIVE DIS New quark distribution function	$\vec{e}p(D) \rightarrow e(M,\gamma)X$ $\vec{e}\vec{p}(\vec{D}) \rightarrow e(M,\gamma)X$ $\vec{e}p^T \rightarrow e(M,\gamma)X$	PDF, TMD, d, $\bar{u}$ Frag. distribution fun. Transversity	Large t coverage Low $L \rightarrow$ large acc. pol. targets
FORM FACTOR AND GPDs, and BARYONS SPECTROSCOPY	$\vec{e}D \rightarrow e(n,p)$ $\vec{e}p \rightarrow eN(\pi^0,\pi^+)$ $\vec{e}p \rightarrow eN(\eta,\pi^+\pi^-,etc)$	Neutron magnetic FF $E_{1+}/M_{1+}, S_{1+}/M_{1+}$ $N\Delta, NN^*$, FF	Detection of n and p Full coverage Multiparticle detection

Table 2.2: **HALL B 12 GEV PHYSICS PROGRAM SUMMARY - QCD PROPERTIES**
The color code indicates reactions that will be measured simultaneously in CLAS^{++}

PHYSICS PROGRAM	**REACTION(s)**	**PHYSICS QUANTITY**	**REQUIREMENTS**
QCD PROPERTIES			
Space-time characteristics of hadronization (DIS kinematics)	$\vec{e}\,^{2}H \rightarrow e\ hadron\ X$ $\vec{e}\,^{14}N \rightarrow e\ hadron\ X$ $\vec{e}\,^{56}Fe \rightarrow e\ hadron\ X$ $\vec{e}\,^{84}Kr \rightarrow e\ hadron\ X$ $\vec{e}\,^{197}Au \rightarrow e\ hadron\ X$ $hadron = \pi^0, \pi^+, \pi^-, \eta, \omega, \eta', \phi, K^+, K^-, K^0, p, \bar{p}, \Lambda, \Lambda(1520), \Sigma^+, \Sigma^0, \Xi^0, \Xi^-$	Hadronization length vs. Q^2, ν, p_T, z, hadron mass and size, and quark flavor; quark energy loss, gluon emission properties, quark-gluon correlations.	Direct hadron ID for neutral and charged hadrons; Multi-particle detection Central detector
Color transparency in coherent vector meson production	$\vec{e}\,^{2}H \rightarrow e\ ^{2}H\rho$ $\vec{e}\,^{2}H \rightarrow e\ ^{2}H\omega$ $\vec{e}\,^{2}H \rightarrow e\ ^{2}H\phi$	Onset of color transparency	Multi-particle detection charged hadron ID
Color transparency in ρ production from complex nuclei	$\vec{e}\,^{2}H \rightarrow e\ \rho\ X$ $\vec{e}\,^{14}N \rightarrow e\ \rho\ X$ $\vec{e}\,^{56}Fe \rightarrow e\ \rho\ X$	Color transparency at fixed coherence length	Multi-particle detection charged hadron ID
Color transparency in quasielastic scattering	quasielastic e,e'p on $^{2}H, ^{14}N, ^{56}Fe, ^{84}Kr, ^{197}Au$	Color transparency	Multi-particle detection
Structural modifications of bound nucleons	$\vec{e}\,^{2}H \rightarrow e\ p\ X$	Structure function of bound neutrons	Multi-particle detection Central detector

Table 2.3: **CLAS^{++} PROGRAM SUMMARY - PHYSICS NEAR REAL PHOTON LIMIT**
The color code indicates reactions that will be measured simultaneously.

PHYSICS PROGRAM	**REACTION(s)**	**OBSERVABLES**	**REQUIREMENTS**
MESON SPECTROSCOPY	$\text{“}\vec{\gamma}\text{”}{}^4He \rightarrow {}^4He\pi^0\eta(\eta\prime)$ $\text{”}\vec{\gamma}\text{”}p \rightarrow p(n\pi)$ $\text{”}\vec{\gamma}\text{”}p \rightarrow p(n\pi k)$	Search for $J^{pc} = 1^{-+}$ exotics	-Forward angle electron detector -Large acceptance for photons -Thin target for low energy recoils -Lage acceptance for multi-pions and kaons
LARGE ANGLE COMPTON SCATTERING	$\text{”}\vec{\gamma}\text{”}p \rightarrow p\pi^0$	Pion GPDs	-Forward angle electron detector -Large acceptance for photons